Journal of Geophysical Research Solid Earth

Supporting Information for

Along-Trench Structural Variations of the Subducting Juan de Fuca Plate from Multichannel Seismic Reflection Imaging

Shuoshuo Han[1,2,3]*, Suzanne M. Carbotte[1], Juan Pablo Canales[4], Mladen R. Nedimović[5,1], Hélène Carton[6,1]

[[1] Lamont-Doherty Earth Observatory, Palisades, NY, USA; [2] Department of Earth and Environmental Sciences, Columbia University, New York, NY, USA; [3] Now at Institute for Geophysics, The University of Texas at Austin, Austin, TX, USA; [4] Woods Hole Oceanographic Institution, Woods Hole MA, USA; [5] Department of Earth Sciences, Dalhousie University, Halifax, NS, Canada; [6] Institut de Physique du Globe de Paris, Paris, France

*Corresponding author contact information: han@ig.utexas.edu]

Contents of this file

Text S1, S2
Figures S1, S3, S4
Table S1, S2

File Uploaded Separately

Figures S2

Introduction

This supporting information provides detailed description of the independent dip-moveout based processing flow that aims to eliminate contamination from out-of-plane arrivals and validate the nature of the intra-crustal/mantle reflectivity (Text S1, Figs. S1, S3, Table S1), estimation of maximum magnitude of outer-rise earthquakes (Text S2, Table S2), un-interpreted pre-stack time migrated image of the MARGIN transect (Fig. S2), and calculation of the range of apparent dips of subduction bending faults and lower crustal ridgeward dipping reflections (Fig. S4).

Text S1 Processing and analysis to aid interpretation of crustal/mantle dipping events

2D MCS images are subject to contamination by out-of-plane scattering of seismic energy. Scattering from isolated point scatters (e.g. rough seafloor or basement) may increase the background noise level and result in over-migration smiles on migrated images. Scattering from fault scarps at the seafloor or at basement beneath the sediments can give rise to linear events that may be misinterpreted as true crustal/mantle structure, especially when the strike of the seismic line is at a low angle with that of the nearby faults [*Kent et al.*, 1996]. As out-of-plane reflections travel through a medium of lower average velocity compared with true crustal/upper mantle reflections, this energy is not well focused at crustal depths through pre-stack time migration (PSTM). Therefore, the dipping events on our PSTM image should be genuine crustal/upper mantle reflections. To further confirm this, we also apply dip-moveout (DMO) with FK filtering and post-stack time migration as used in previous studies of oceanic crust to remove side-scattering from the seafloor and basement relief [*Calvert*, 1995; *Ranero et al.*, 1997; *Reston et al.*, 1999; *Canales et al.*, 2005]. Through this processing, we test the possibility that some of the dipping events arise from out-of-plane scattering from the seafloor at the deformation front, and from the abyssal hill faults offsetting the top of oceanic crust and buried by sediments.

(1) Seafloor related out-of-plane energy

In the vicinity of our survey line, the seafloor is generally flat and smooth; the only linear features that may scatter back seismic energy are the fault scarps in the accreted sediments on and beyond the deformation front. From distance ~2-342 km, the deformation front is more than 10 km away from our survey line and seafloor scattering events are predicted to arrive at travel times later than 12.288s, which is the length of our record (Fig. S1). Therefore side-scattering from fault scarps on the seafloor may only contaminate the crust/mantle of the southernmost 40 km of the line.

Out-of-plane scattering from the seafloor can arrive at TWTTs that overlap with crust/mantle reflections and with moveout smaller than that of seafloor reflection but similar to that of

crustal/mantle reflections on CMP gathers (i.e. with apparent velocity higher than water velocity and closer to crustal/mantle velocity). The application of DMO following NMO with water velocity will increase the moveout of out-of-plane scattering events to similar to that of seafloor reflections, therefore increasing the differential moveout between seafloor-scattering and crust/mantle reflections. The out-of-plane energy with adjusted moveout can then be removed using f-k filtering. The filtered data are then stacked and migrated with true velocities (Table S1).

We compare the post-stack migrated images with and without the DMO-based processing sequence (Table S1), as shown in Fig. S3a-b. The abundance, location, depth, and dips of the linear events in the crust/mantle are very similar. No linear events are removed after the DMO-based processing, indicating that the linear events on the crust/mantle section do not reflect seafloor scatterers. The amplitude of sediment reflections is reduced on Fig. S3b because low velocity sediment reflections have move-outs more similar to seafloor reflections compared with crust/mantle reflections, and thus some of the near offset signal is removed by f-k filtering.

Table S1 DMO-based approach to eliminate out-of-plane-scattering

Process	**Explanation**
1. Reassign offset in CDP gathers to designate offsets at 75 m spacing.	This step is to prepare the data for DMO, which is applied on common offset gathers.
2. NMO (Water velocity or the RMS velocity of basement)	After NMO with water velocity, seafloor reflection events on the CDP gathers are flattened. However, the out-of-plane seafloor scattering, which has an apparent higher-than-water velocity and smaller moveout, will be over-corrected.
3. DMO	After DMO, the moveout of out-of-plane scattering is adjusted to water-velocity moveout, thus the events appear to be flat on CDP gathers.
4. f– k filter (-2 to + 2 ms/trace)	An fk-filter is applied to eliminate the flattened events (events that would stack best at water velocity), i.e. in-and out-of-plane scattering from the seafloor is eliminated from the CDP gathers.
5. Remove NMO (Water velocity or the RMS velocity of basement)	The moveout of all the other sub-surface events are restored.
6. Stacking using realistic stacking velocity	The cleaned data are stacked with realistic velocity.
7. Kirchhoff post-stack time migration with realistic velocity	The cleaned data are migrated with realistic velocity.
8. Time varying gain for display purpose	

(2) Basement related out-of-plane energy

Scarps of abyssal hill faults offsetting basement may also give rise to linear dipping events in the crust/mantle section [*Kent et al.*, 1996]. With more than 2 km of sediment on top of the oceanic

crust in our study region, the location and length of these fault scarps near our survey line cannot be determined. We apply the DMO-based approach (Table S1) using basement RMS velocity (2100-2400 m/s) as the NMO velocity and compare the resulting post-stack migrated images with conventional post-stack migrated images (Fig. S3c-f). Basement reflections and scattering are removed, and the background noise level of the crust (especially the upper crust) is reduced, making some events more prominent. For example, within PW3, the upper crust is greatly cleaned, and one southward dipping event and one northward dipping event at 5900-6400 ms become apparent (Fig. S3e-f). Most of the crustal and upper-mantle dipping events remain after this processing, confirming that they are genuine crustal/upper mantle reflections.

There are a couple of dipping events that are potentially out-of-plane reflections and are removed through this processing. Near propagator wake PW3 where the basement is relatively rough in comparison to the rest of the line, a shallowly dipping event at 6000 ms is removed along with the over migrated events at 6200-6700 ms, which may arise from isolated point scatters from out-of the plane rough basement (Fig. S3e-f). Another example is near the seamount at 80 km where one strong dipping event that extends from the base of the seamount to 500 ms beneath the basement is removed (Fig. S3c-d). This event could be generated from out-of-plane seamount topography. On the other hand, as the true reflections in the uppermost upper crust have similar velocity as the basement, the approach described above may remove some of the near-offset signal of these reflections. Therefore it is also possible that this event is a fault in the shallow crust beneath the flank of the seamount.

Text S2 Estimation of maximum magnitude of outer-rise earthquakes in the Juan de Fuca plate

We estimate the maximum magnitude of outer-rise earthquakes offshore Washington and Oregon using fault geometry and fault throw information obtained from Ridge-to-Trench data [*Han et al.*, 2016]. As the incoming JdF plate is covered by a thick sediment layer, the lengths of bending

faults cannot be determined from bathymetry directly. Here we assume two fault lengths (50 km and 20 km) based on observations from sediment-poor margins with relatively young incoming oceanic plates [*Masson*, 1991; *Ranero et al.*, 2003]. When the spreading fabrics of the oceanic crust are sub-parallel to trench, abyssal hill faults are reactivated under subduction bending, and the length of bending faults is similar to that of abyssal hill faults (50 km is assumed for this case). When the spreading fabrics are at high-angle with trench, new normal faults that are sub-parallel to the trench are formed and these faults may have shorter lengths (20 km is assumed for this case). The depth extent of faults is estimated from the depth range where fault plane reflections are imaged in the crust and uppermost mantle (13 km and 3 km for Oregon and Washington respectively). Fault dips of 40-60˚ and 60-65˚ are used for faults offshore Oregon and Washington [*Han et al.*, 2016]. An average shear modulus of 45 GPa is used for oceanic crust.

The largest uncertainty is associated with the estimation of slip during earthquakes. Within 75-80 km seaward of the deformation front offshore Oregon and 65-70 km offshore Washington, the JdF plate is deformed due to sediment loading and subduction bending. The average fault throw increases from 17 m to 100 m (max 124 m) from distance 75 km to 0 km seaward of the deformation front along OR transect over time of 2.6786 Myr (28 mm/yr spreading rate) [*Han et al.*, 2016]. Assuming that the bending-related elastic energy stored in the oceanic plate during one megathrust earthquake cycle is released in one major outer-rise earthquake following a megathrust earthquake, ~5357 (300 yr recurrence interval)-8929 (500 yr recurrence interval) outer-rise earthquakes occurred during this time period with average slip of 0.0093 to 0.02 m. Similarly, average fault throw increases from 19 m to 22 m (max 46 m) within 65 km seaward of the deformation front over a time period of 2.3214 Myr (28 mm/yr spreading rate) [*Han et al.*, 2016], the average slip of outer-rise earthquakes with 300-500 yr recurrence intervals are 0.00039-0.0058 m.

Using equation (*), the maximum magnitude of outer-rise earhtuqkaes offshore of Oregon and Washington is calculated to be Mw 4.0-5.0 and Mw 5.3-5.9 respectively (Table S2).

$$Mw = \frac{2}{3}\log\left(\frac{\mu \cdot L \cdot D \cdot s}{\sin(\theta)}\right) - 6.06 \quad (*)$$

Where μ is shear modulus, L and D are the length and depth extent of faults, θ is fault dip, s is slip.

As the bending-related elastic energy may be released by many smaller outer-rise earthquakes distributed throughout the megathrust earthquake cycle, our estimation represents the high-end of the outer-rise earthquake magnitude in this region.

Table S2 Parameters of outer-rise faults used for calculation of maximum earthquake magnitude

	Fault Length (km)	Fault Depth (km)	Fault Dip	Shear Modulus (GPa)	Max Slip per Earthquake (m)	Maximum Earthquake Magnitude
Oregon	50	13	40-60°	45	0.0093-0.02	5.6-5.9
	20					5.3-5.6
Washington	50	3	60-65°	45	0.00039-0.0058	4.2-5.0
	20					4.0-4.8

References

Calvert, A. J. (1995), Seismic evidence for a magma chamber beneath the slow-spreading Mid-Atlantic Ridge, *Nature*, *377*(6548), 410.

Canales, J. P., R. S. Detrick, S. M. Carbotte, G. M. Kent, J. B. Diebold, A. Harding, J. Babcock, M. R. Nedimović, and E. Van Ark (2005), Upper crustal structure and axial topography at intermediate spreading ridges: Seismic constraints from the southern Juan de Fuca Ridge, *J. Geophys. Res.*, *110*(B12).

Han, S., S. M. Carbotte, J. P. Canales, M. R. Nedimović, H. Carton, J. C. Gibson, and G. W. Horning (2016), Seismic reflection imaging of the Juan de Fuca plate from ridge to trench: New constraints on the distribution of faulting and evolution of the crust prior to subduction, *J. Geophys. Res.*, *121*(3), 1849-1872.

Kent, G. M., Kim, II, A. J. Harding, R. S. Detrick, and J. A. Orcutt (1996), Suppression of sea-floor scattered energy using a dip moveout approach - Application to the mid-ocean ridge environment, *Geophysics*, *61*(3), 821-834, doi:10.1190/1.1444007.

Masson, D. G. (1991), Fault patterns at outer trench walls, *Mar. Geophys. Res.*, *13*(3), 209-225, doi:10.1007/bf00369150.

Ranero, C. R., J. P. Morgan, K. McIntosh, and C. Reichert (2003), Bending-related faulting and mantle serpentinization at the Middle America trench, *Nature*, *425*(6956), 367-373, doi:10.1038/nature01961.

Ranero, C. R., T. J. Reston, I. Belykh, and H. Gnibidenko (1997), Reflective oceanic crust formed at a fast-spreading center in the Pacific, *Geology*, *25*(6), 499-502.

Reston, T. J., C. R. Ranero, and I. Belykh (1999), The structure of Cretaceous oceanic crust of the NW Pacific: Constraints on processes at fast spreading centers, *J. Geophys. Res.*, *104*(B1), 629-644.

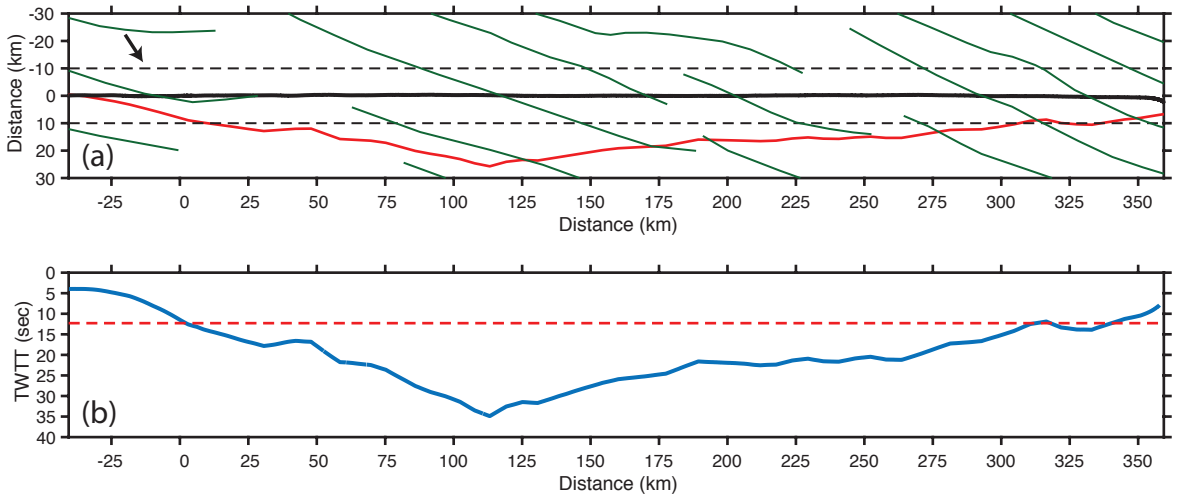

Figure S1 (a) Distance from the MARGIN transect (bold black line) to the deformation front (red line). Black dashed lines mark 10 km seaward and landward of the MARGIN transect. Green lines are isochrones. Black arrow indicates convergence direction of the JdF plate with respect to the North America plate. (b) Predicted arrival time in TWTT of scattered energy from deformation front fault scarps (blue line). The red dashed line indicates the record length of the data (12.28 sec TWTT).

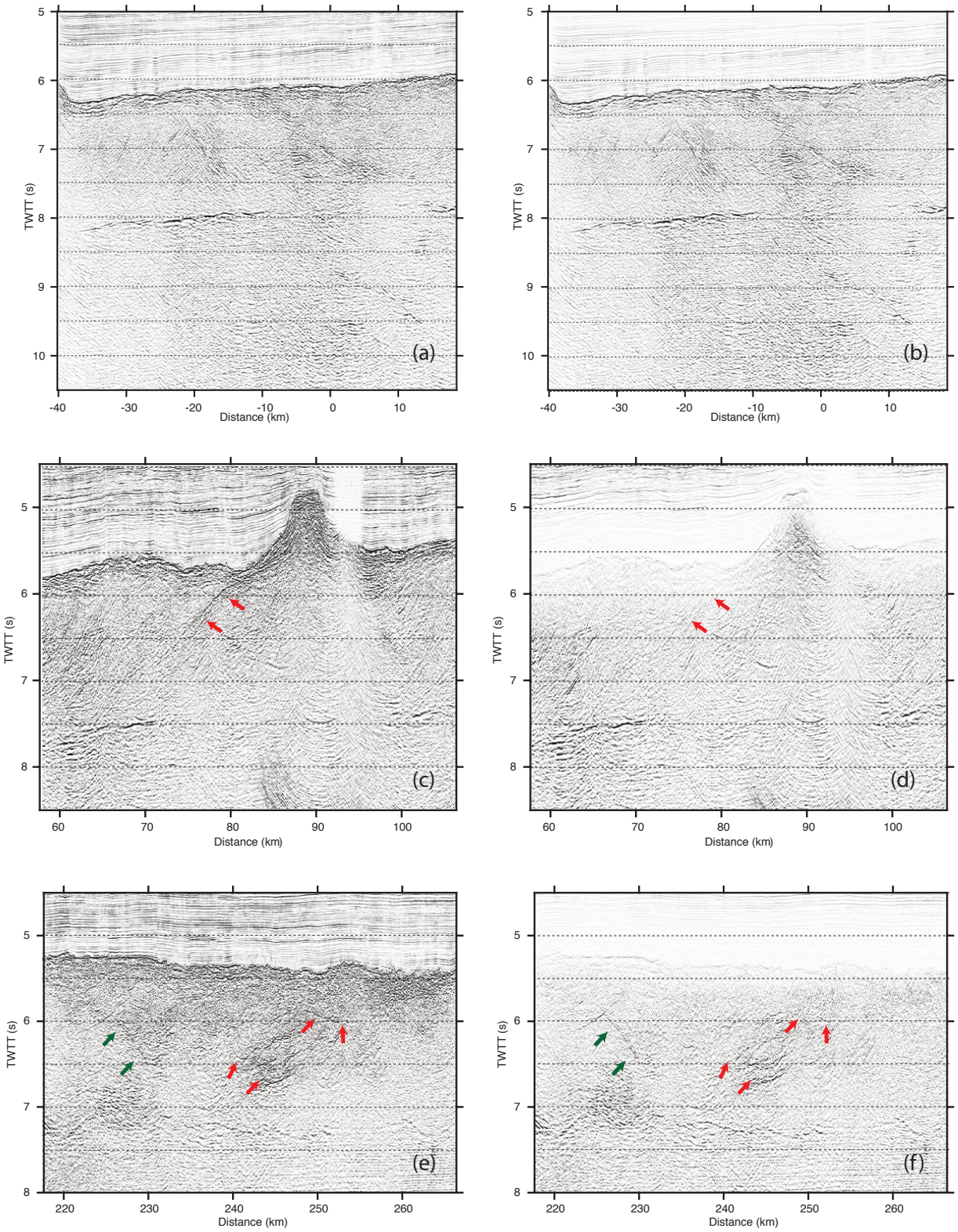

Figure S3. DMO analysis for intracrustal reflections. (a) and (b) Post-stack migrated sections within crustal segment 1 without and with DMO (using water velocity and FK filtering) respectively. Little change is evident in the crustal reflections after DMO. (c) and (d) Post-stack migrated sections within crustal segment 2 without and with DMO (using basement velocity and FK filtering) respectively. One dipping reflector (indicated with red arrows) near the seamount is removed by this process and may be an out-of-plane artifact. (e) and (f) Post-stack migrated sections within PW3 without and with DMO (using basement velocity and FK filtering) respectively. Note that near basement noise level is reduced after this process and some dipping events become more apparent (indicated with green arrows). One dipping reflector and some over-migration noise (indicated with red arrows), which is likely sourced from out-of-plane, is removed. Vertical exaggeration is ~13.3 at seafloor.

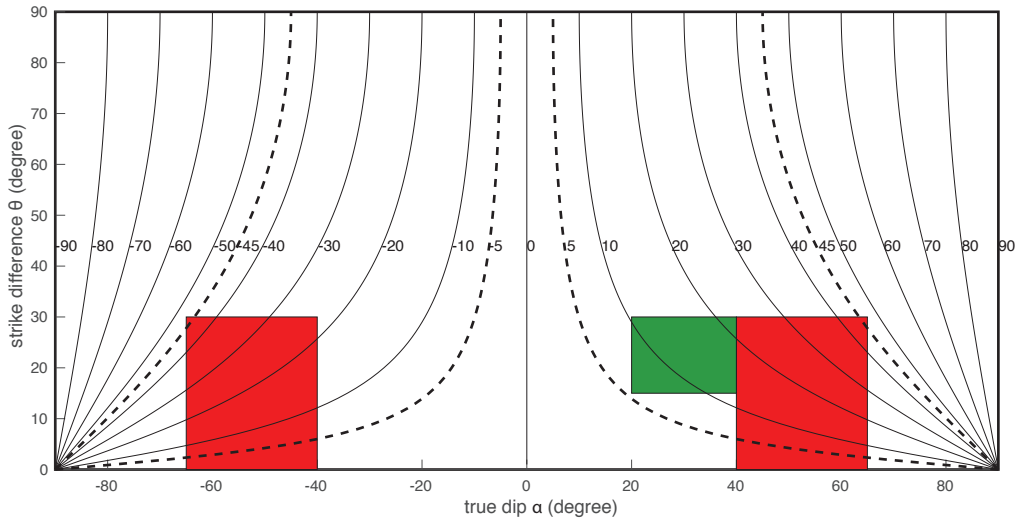

Figure S4 Predicted apparent dips (ϒ) on a 2D seismic line with given true dips (α) and strike difference (θ) between the dipping plane and seismic profile. The red squares are the range of strike differences and true dips expected for spreading perpendicular abyssal hill faults. The green rectangle is the range of strike differences and true dips for lower crustal reflections (LCRs).